High Resolution Structure, Stability, and Synaptotagmin Binding of a Truncated Neuronal SNARE Complex*

James A. Ernst and Axel T. Brunger‡

From the Howard Hughes Medical Institute and Departments of Molecular and Cellular Physiology, Neurology and Neurological Sciences, and Stanford Synchrotron Radiation Laboratory, Stanford University, Stanford, California 94305

The structure of a truncated SNARE complex has been solved to 1.4-Å resolution revealing a stabilizing salt bridge, sites of hydration, and conformational variability of the ionic central layer that were not observed in a previously published structure at 2.4-Å resolution (Sutton, R. B., Fasshauer, D., Jahn, R., and Brunger, A. T. (1998) *Nature* 395, 347–353). The truncated complex lacks residues involved in phospholipid binding and denatures at a lower temperature than longer complexes as assessed by SDS and circular dichroism thermal melts. The truncated SNARE complex is monomeric, and it retains binding to synaptotagmin I.

Members of the conserved family of SNARE[1] proteins play an important role in protein-assisted vesicle membrane fusion (1–7). SNARE complex formation juxtaposes synaptic vesicle and plasma membranes and thus may set the stage for vesicle membrane fusion. In the final stages of fusion, neurotransmitter release is probably regulated by the Ca^{2+}-binding protein synaptotagmin (8). Each SNARE protein contains at least one core domain that binds to other SNARE proteins to form a four-helix bundle (8). This four-helix bundle is composed of 16 layers transverse to the helical axes including a buried ionic layer at the center of the four-helix bundle (9).

The neuronal SNARE complex consists of three SNAREs: synaptobrevin, syntaxin, and SNAP-25 (Synaptosome-associated protein, 25 kDa) (Fig. 1). Synaptobrevin (also referred to as vesicle-associated membrane protein) is a 12-kDa protein with a SNARE binding domain and a single spanning transmembrane domain (10, 11). Syntaxin is a 35-kDa protein with a three-helix bundle regulatory domain, a SNARE binding domain, and a single spanning transmembrane domain (1, 3, 12, 13). SNAP-25 is a 25-kDa protein with two SNARE binding domains and a linker domain of ~45 amino acids. SNAP-25 is targeted to the plasma membrane by its association with syntaxin via palmitoylation of three cysteine residues in the linker domain (14, 15).

The crystal structure of the neuronal SNARE complex revealed a conserved buried ionic layer at the center of the four-helix bundle (9) whose function is still uncertain (16). Most probably, it plays a role during *N*-ethylmaleimide-sensitive factor (NSF) driven disassembly of the SNARE complex, because mutations of this central layer can disrupt this process (17).

Here we present the crystal structure of the neuronal SNARE complex at a 1.4-Å resolution. To obtain this high resolution crystal structure, the individual SNAREs were truncated in comparison with the corresponding constructs used in the previously published crystal structure solved at a 2.4-Å resolution (9). This high resolution structure reveals new sites of hydration and stabilizing intermolecular interactions. We further characterize the thermal stability of this SNARE complex by CD and SDS melts, its oligomerization state, and its binding properties to synaptotagmin in the presence of Ca^{2+} and EDTA.

MATERIALS AND METHODS

Constructs

Constructs encoding sequences for the "minimal" complex (Fig. 1), rat syntaxin 1a residues 180–262 (SXa), synaptobrevin II residues 1–96 (SBa), SNAP-25 B residues 1–83 (SN1a), and SNAP-25 B residues 120–206 (SN2a) were described elsewhere (18). The cDNA-encoding sequences for the N-terminally truncated minimal complex and the microcomplex (Fig. 1), rat syntaxin 1a residues 188–262 (SXb) and residues 191–256 (SXc), synaptobrevin II residues 25–96 (SBb) and residues 28–89 (SBc), SNAP-25 B residues 7–83 (SN1b), and SNAP-25 B residues 132–204 (SN2b) and 141–204 (SN2c) were subcloned from these constructs into the expression plasmid pET28a (Novagen) or pGEX-2T (Amersham Biosciences) (SN2b only). The cDNA encoding the sequence for rat synaptotagmin I-(139–421) were subcloned from synaptotagmin I cDNA into the pGEX-2T expression vector. The G374 sequence variant of synaptotagmin (19) was generated using the QuikChange mutagenesis kit (Stratagene) using the oligomers 5′-TG-TAACCAACGAAGACTTTGCCGATGGCGTCGTTCTTGCC-3′ and 5′-GGCAAGAACGACGCCATCGGCAAAGTCTTCGTTGGTTACA-3′. The correct sequences of all of the constructs were verified by DNA sequencing (Biocore Inc., Palo Alto, CA, or Keck facility, Yale University, New Haven, CT).

The pET28a expression plasmids were transformed into *E. coli* BL21(DE3) competent cells using standard protocols (20). Cells were grown at 37 °C in a BIOFLO 3000 fermentor (New Brunswick, NJ) using ECPYM1 medium (21) in the presence of 50 $\mu g/ml$ kanamycin sulfate. The expression was induced with 1 mM isopropyl-1-thio-β-D-galactopyranoside at an A_{600} of 20. The pGEX-2T expression plasmids were transformed into *E. coli* BL21-competent cells using standard protocols. Cells were grown at 37 °C in terrific broth supplemented with 100 $\mu g/ml$ ampicillin media in 4-liter flasks. At an A_{600} of ~1, the temperature was reduced to 25 °C and expression was induced for 3 h using 1 mM isopropyl-1-thio-β-D-galactopyranoside. Approximately 3 h after induction, cells were harvested by centrifugation for 20 min at 4200 rpm in a Beckman J6-HC Centrifuge using a JS-4.2 rotor. Cells were immediately frozen in liquid nitrogen and stored at −80 °C.

Cells containing histidine-tagged SNARE proteins were resuspended in 1:10 denaturing lysis buffer (7 M guanidine, 50 mM Tris, pH 8.2, 10

[1] The abbreviations used are: SNARE, soluble *N*-ethylmaleimide-sensitive factor attachment protein receptor; SNAP-25, Synaptosome-associated protein, 25 kDa; GST, glutathione *S*-transferase; DTT, dithiothreitol; MALLS, multi-angle laser light scattering; MPD, (±)-2-methyl-2,4-pentanediol; MES, 4-morpholineethanesulfonic acid.
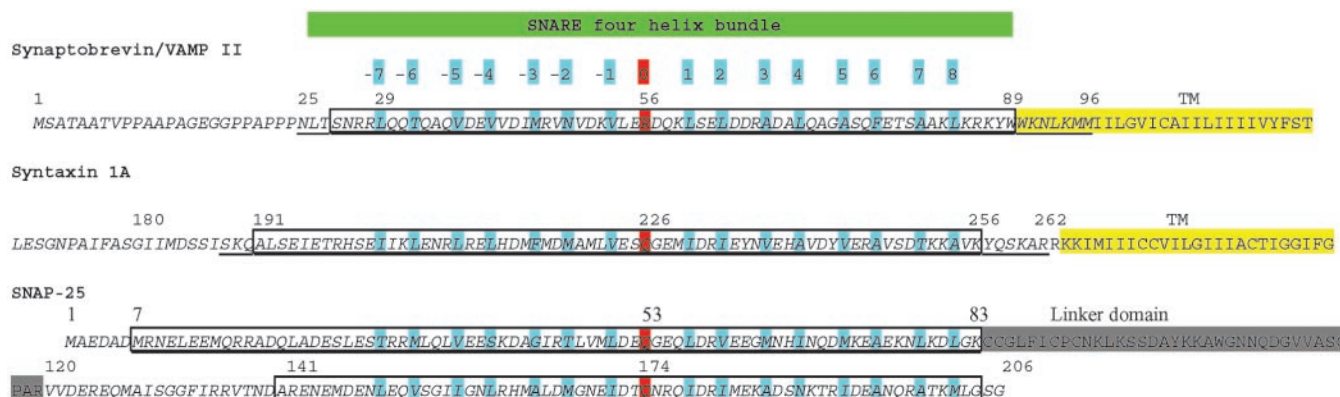
FIG. 1. **Sequence alignment of neuronal SNAREs.** The sequence for the constructs used for the 2.4-Å crystal structure of the minimized complex (9) is shown in *italics*. In text, they are referred to as constructs SBa, SXa, SN1a, and SN2a. The N-terminal truncations of these constructs are *underlined*. In text, they are referred to as constructs SBb, SXb, SN1b, and SN2b. The constructs of the microcomplex are indicated by *boxes*. In the text, these constructs are referred to as SBc, SXc, SN1b, and SN2c. Hydrophobic layers of the SNARE complex are shown in *blue*, and the ionic central (*zero*) layer is shown in *red*. Sequences displayed are rat synaptobrevin II (gi:6981613), rat syntaxin-1A (gi:207126), rat SNAP-25 B (gi:2116627).

mM imidazole) and passed once through a Microfluidizer (Microfluidics) at 25,000 p.s.i. Cell lysate was cleared by ultracentrifugation in a Beckman Optima XL-100K Centrifuge using a type 45 rotor at 45,000 rpm for 45 min. Cleared lysate was loaded in bulk for 10 h onto 25-ml nickel-nitrilotriacetic acid resin (Qiagen). The column was washed with 10-column volumes of denaturing wash buffer (6 M guanidine, 50 mM Tris, pH 8.2, 20 mM imidazole) followed by 10-column volumes of native buffer (300 mM NaCl, 20 mM Tris, pH 7.7, 20 mM imidazole). The protein was then eluted with 3-column volumes of native buffer containing imidazole at 250 mM.

Cells containing glutathione *S*-transferase (GST)-tagged synaptotagmin I C_2AB and SN2b were resuspended in 300 mM NaCl, 50 mM NaH_2PO_4, 50 mM Tris, 1 mM EDTA, 5 mM DTT, 0.5 mM phenylmethylsulfonyl fluoride, 1 mg/ml leupeptin, 1 mg/ml pepstatin, 10 mM benzamidine, and 100 mg/ml DNase. Cells were lysed by disruption using a Microfluidizer with two passes at 25,000 p.s.i. Cell lysate was cleared by ultracentrifugation in a Beckman Optima XL-100K Centrifuge using a type 45 rotor at 45,000 rpm for 45 min. Cleared lysate was loaded in bulk for 4 h onto 25 ml of glutathione resin (Amersham Biosciences) and washed with 10-column volumes of buffer. Protein was eluted with 15 mM glutathione and dialyzed overnight into 200 mM NaCl, 20 mM HEPES pH 7.8, 5 mM DTT, and 1 mM EDTA. Synaptotagmin was further purified using fast protein liquid cation exchange chromatography over a Mono S 10/10 column (Amersham Biosciences).

The concentration of the proteins was calculated by using a Bradford assay or UV absorption at 280 nm. UV spectra demonstrated that synaptotagmin was free of the DNA contamination mentioned elsewhere (19).

The SNARE complex was formed by mixing SNAP-25, synaptobrevin, and syntaxin fragments at a 1:1:1:1 ratio, mixed with 4 M urea to prevent precipitation, and dialyzed into 100 mM NaCl, 20 mM Tris, pH 8.2, and 1 mM $CaCl_2$ at 4.0 °C. Thrombin was added after 4 h to remove the histidine tags from the proteins, and dialysis was continued for 10 h. SNARE complex was purified on a Mono Q 10/10 anion exchange column where it eluted between 230 and 330 mM NaCl. Final size exclusion purification was performed using a Superdex 200 16/60 column (Amersham Biosciences).

The purity of the SNARE complex was assayed by SDS-PAGE using Phast gels (Amersham Biosciences) and Coomassie Blue staining. Final fractions containing completely formed SNARE complex were pooled, and the protein concentration was determined by UV absorption at 280 nm. The complex was flash-frozen in liquid nitrogen and stored at −80 °C.

Biochemistry

CD—CD experiments were performed on a Aviv 62DS spectrometer at 150 mM NaCl, 20 mM Na_2HPO_4, pH 7.8, and 10 μM SNARE complex. Temperature scans were performed between 37 and 97 °C at two-degree intervals with 1-min equilibration between temperature changes and 1-min acquisitions with data averaging at each temperature point.

GST Pull-down Assays—GST pull-down experiments were performed at room temperature in 150 mM NaCl with 20 mM HEPES, pH 7.8, and 1 mM DTT in the presence of either 0.5 mM $CaCl_2$ or 1 mM EDTA. Samples were mixed at room temperature, incubated for 1 h

with GST beads, and washed three times with buffer and mixed with SDS sample loading buffer. The samples were analyzed by SDS-PAGE using 10–25% SDS Phast gels.

Multi-angle Laser Light Scattering (MALLS)—Size exclusion chromatography was performed using a Superdex 200 10/30 column at a flow rate of 0.5 ml/min. Measurements were performed in 150 mM NaCl, 10 mM HEPES, pH 7.8, and 5 mM DTT. The elution profile was monitored by UV absorption at 280 nm, light scattering at 690 nm, and differential refractometry. Light scattering and differential refractometry were carried out using the Dawn and OptiLab instruments (Wyatt Technology). Analysis was carried out using the Astra software (22). For each sample, 100 μl of protein at 1 mg/ml protein was loaded. The differential refractive index increment (dn/dc) is fairly constant for proteins and was set to 0.185.

Crystallography

Crystallization—Crystallization trials were conducted using the hanging drop vapor diffusion method. The initial SNARE protein concentration was 9 mg/ml in a solution of 200 mM NaCl, 10 mM HEPES (Fluka), pH 7.8, and 5 mM DTT (American BioAnalytical). Crystals appeared at 4 °C in 1–3 days and grew to full size in 3–5 days. The well solution contained 15–20% (±)-2-methyl-2,4-pentanediol (MPD) (Fluka), 75–125 mM $CaCl_2$ (Fluka), and 50 mM MES (Fluka) at pH 5.0–6.0. Initial drops consisted of a one-to-one mixture of protein sample and well solution resulting in a total volume of 4 μl. The crystals grew in clusters as thick needles. To obtain single crystals, these clusters of crystals were used for streak seeding into preequilibrated hanging drops. Single crystals were prepared for freezing by serial transfer using nylon loops into mother liquor with increasing amounts of MPD as a cryoprotectant up to 55%. Crystals were then frozen by rapid transfer directly into liquid nitrogen.

Diffraction Data—Diffraction data were collected at the Lawrence Berkeley National Laboratory Advanced Light Source beamline BL 8.2.1 from a single crystal in one pass at 100 K using an Area Detector System Quantum 210 2 × 2 CCD detector. The diffraction data were collected to a 1.4-Å resolution. All of the data processing was carried out using the programs Denzo and Scalepack (23). Statistics of the diffraction data are shown in Table I. The crystals formed with one copy of the SNARE complex per asymmetric unit in space group $P2_12_12_1$.

Phases—The phases for the diffraction data were obtained by molecular replacement using the direct rotation search (24) as implemented in the program CNS (version 1.1) (25) using diffraction data from 20 to 3.5-Å resolution. The subsequent translation function used diffraction data from 15 to 4.0-Å resolution and resulted in an unambiguous solution. The search model consisted of one of the three non-crystallographically related copies of the neuronal SNARE solved at 2.4 Å (9). It was truncated to contain only those residues present in the microcomplex.

Model Building—Model building was performed using the program O (26). The initial model was optimized by rigid body refinement followed by simulated annealing with torsion angle dynamics (27), restrained *B*-value refinement (28), and conjugate gradient minimization using the MLF target function (29). Overall anisotropic scale factors and bulk solvent correction were applied to the diffraction data. The progress of model rebuilding and refinement was monitored by cross-
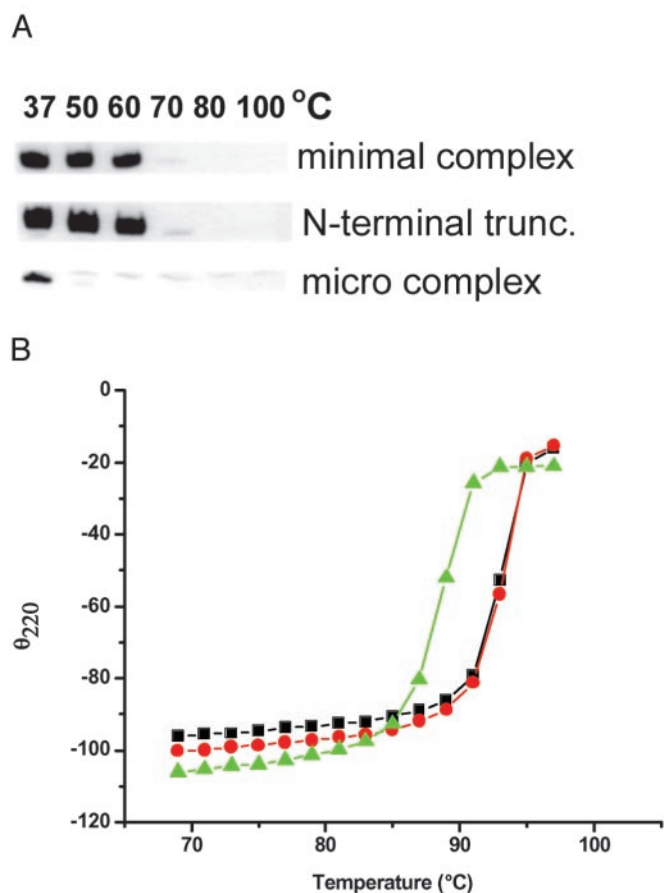
A

B

FIG. 2. **Stability of SNARE complexes.** *A*, SDS stability of the minimal complex, the N-terminally truncated minimal complex, and the microcomplex. Experiments were performed as described previously (43). SNARE complex was mixed with SDS to a final concentration of 0.67%, heated at the indicated temperature for 5 min, and immediately run on a 10–15% SDS-PAGE gel. *B*, CD thermal melts of SNARE complexes as monitored at 220 nm. The minimal SNARE complex is shown in *blue*, the N-terminal truncation of the minimal SNARE complex is shown in *red*, and the microcomplex is shown in *green*.
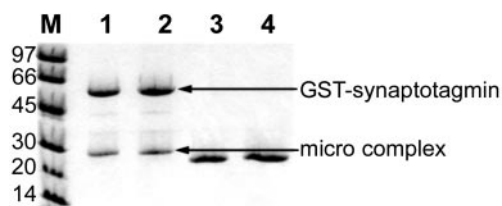

FIG. 3. **Synaptotagmin I binding of microcomplex.** Shown is a GST pull-down assay of the micro-SNARE complex using the GST-tagged C_2AB fragment of synaptotagmin I (residues 139–421). In each lane, 2 μM microcomplex was incubated with 2.0 μM GST-synaptotagmin I C_2AB (*lanes 1* and *2*) or 2 μM GST alone (*lanes 3* and *4)* and glutathione resin. Experiments were performed in the presence of 0.5 mM Ca^{2+} (*lanes 1* and *3*) or 1 mM EDTA (*lanes 2* and *4*). The microcomplex is indicated by an *asterisk*, and GST-synaptotagmin is indicated by an *arrow*.

validation using R_{free} (30), which was computed from a randomly chosen test set comprising 10% of the data. The sites of hydration were placed by inspection of peaks larger than three standard deviations above the mean in $F_o - F_c$ σ_A-weighted electron density maps. Only those sites were kept that exhibited reasonable protein solvent hydrogen-bonding distances without steric conflict and whose *B*-value refined to <55 Å^2. MPD and Ca^{2+} were identified by inspection of $F_o - F_c$ and $2F_o - F_c$ σ_A-weighted electron density maps. At various points during refinement, σ_A-weighted, annealed $2F_o - F_c$ composite omit maps were used to minimize the effects of model bias. All of the refinements were carried out using the program CNS (25). Statistical linear least-squares superposition of the structures was performed using the LSQMAN (31)

TABLE I
Data statistics

Average multiplicity is 5.5.

Resolution range	Unique reflections	I/Σ(I)	Completeness	R_{merge}[a]
100.00–3.12	5213	23.7	98.5	0.050
3.12–2.48	5015	23.7	100.0	0.060
2.48–2.17	4980	21.2	100.0	0.077
2.17–1.97	4952	17.7	99.9	0.099
1.97–1.83	4919	12.2	99.9	0.154
1.83–1.72	4878	9.2	99.8	0.219
1.72–1.63	4911	6.5	99.8	0.296
1.63–1.56	4814	4.7	98.4	0.374
1.56–1.50	4582	3.7	93.6	0.449
1.50–1.45	4310	3.5	88.4	0.439
All reflections	**48,574**	**20.4**	**97.8**	**0.069**

[a] $R_{\text{merge}} = \Sigma_h \Sigma_j |I_j(\text{h}) - \langle I(\text{h}) \rangle| \Sigma_h \Sigma_j I_j(\text{h})$

TABLE II
Refinement statistics

Space group	$P2_1 2_1 2_1$
Unit cell dimensions	$a = 39.963$ Å, $b = 51.653$ Å,
	$c = 134.407$ Å
	$\alpha = \beta = \gamma = 90°$
Resolution range	34.13–1.45 Å
No. reflection in working set	43,726
No. reflection in test set	4783
R_{cryst} (%)	0.198
R_{free} (%)	0.224
Ramanchandran plot (%)	
Most favored	98.8
Additionally allowed	0.8
Generously allowed	0.4
Disallowed	0.0
No. protein atoms	2206
No. water atoms	322
Average B-factor (Å^2)	27.8

from the Uppsala software factory suite. Graphical images were prepared using PyMOL (Fig. 5) (32) or GRASP (Fig. 4, *a* and *b*) (33).

RESULTS

Oligomeric State of the SNARE Complex—The neuronal SNARE complex has a tendency to oligomerize as shown by analytical ultracentrifugation and MALLS (18). The minimal SNARE complex obtained by limited proteolysis that was used in the 2.4-Å crystal structure had an apparent molecular mass of 60–90 kDa compared with a calculated molecular mass of 41 kDa (18). The C-terminal truncations of synaptobrevin by botulinum toxin B or tetanus toxin produced a monomeric SNARE complex (34). Furthermore, the C-terminal truncation of endobrevin (vesicle-associated membrane protein 8) in the endosomal SNARE complex produced a monodisperse sample (35). Therefore, we truncated the neuronal synaptobrevin at Trp-89 along with the appropriate truncations of syntaxin and SNAP-25 (Fig. 1). These truncations resulted in the removal of approximately one α-helical turn at the C-terminal ends of syntaxin and synaptobrevin (Fig. 1). The truncated neuronal SNARE proteins were then expressed, purified, and assembled. This "micro"-SNARE complex has an apparent molecular mass of 32.5 kDa ± 2% as determined by MALLS (data not shown) compared with a calculated molecular mass of 32.5 kDa. Thus, the microcomplex is both monomeric and monodisperse.

SNARE Complex Stability—We performed temperature-dependent SDS and CD melts of the micro-SNARE complex and compared the results to both the minimal SNARE complex (36) and a SNARE complex that was obtained from the minimal complex by truncation at the N terminus (Fig. 2). Our experiments revealed a roughly 20 °C reduction in the stability of the micro-SNARE complex in SDS relative to both the minimal and N-terminally truncated SNARE complexes (Fig. 2*a*). In light of this reduction in SDS stability, we further investigated the
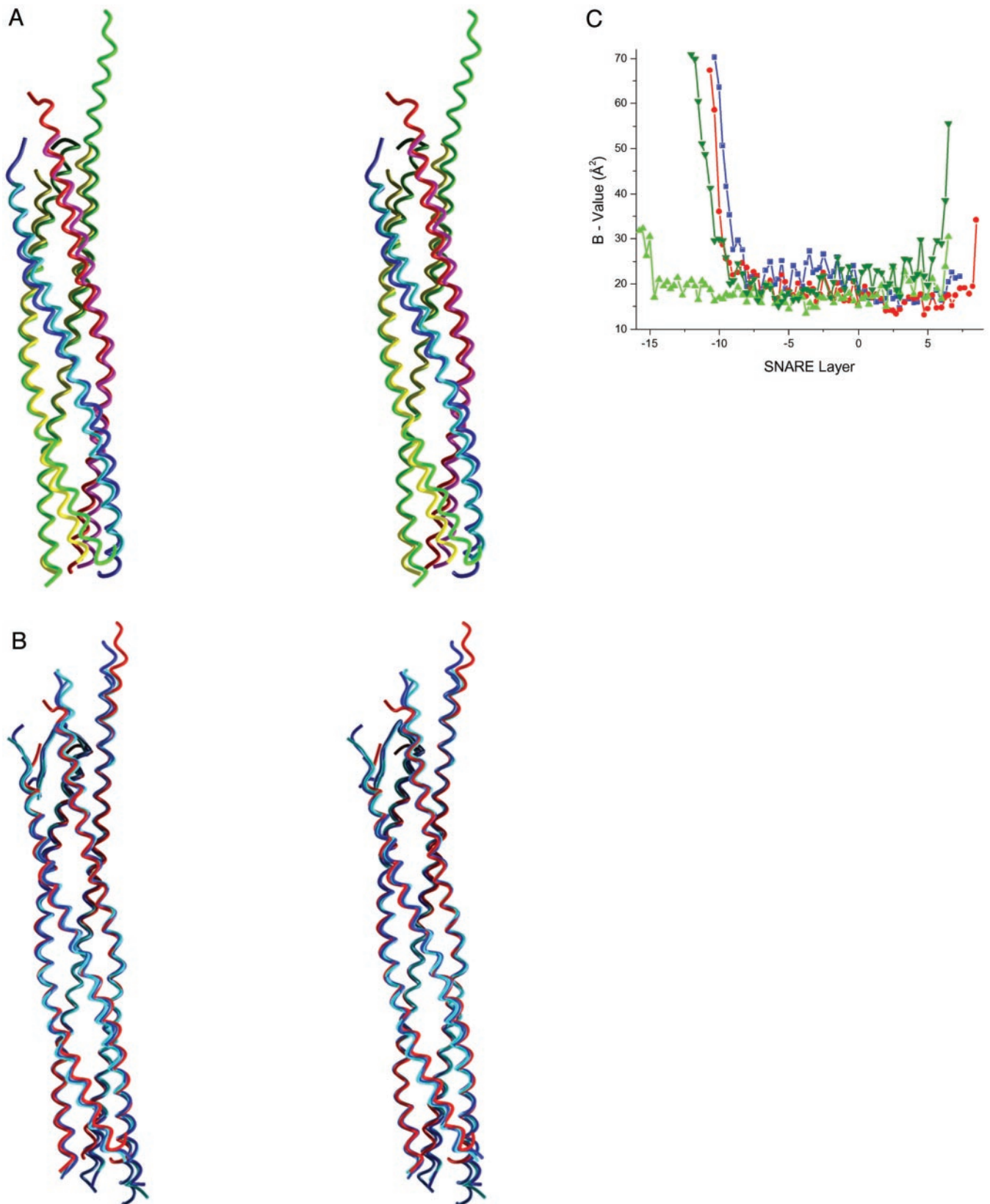
FIG. 4. **Superposition of neuronal and endosomal SNARE complex.** *A*, C$_\alpha$ superposition of the micro-SNARE complex and the endosomal SNARE complex (Protein Data Bank code 1GL2). The color code is as follows: synaptobrevin is shown in *blue*; syntaxin is shown in *red*; SNAP-25 is shown in *green*; endobrevin is shown in *light blue*; vti1b is shown in *magenta*; and syntaxin-8 and syntaxin-7 are shown in *yellow*. *B*, C$_\alpha$ superposition of the micro-SNARE complex with the three complexes in the 2.4-Å crystal structure of the minimal SNARE structure (Protein Data Bank code 1SFC). The color code is as follows: the microcomplex is shown in *red*; the first molecule of the minimal complex crystal structure (chains a–d) (see Ref. 9) is shown in *dark blue*; the second molecule (chains e–h) is shown in *medium blue*; and the third molecule (chains i–l) is shown in *light blue*. *C*, *B*-value plot for the C$_\alpha$ residues of the micro-SNARE complex. The color code is as follows: synaptobrevin is shown in *blue*; syntaxin is shown in *red*; SNAP-25 SN1c is shown in *light green*; and SNAP-25 SN2c is shown in *dark green*.

Superposition was carried out for the neuronal structures (minimal complex and microcomplex) using synaptobrevin residues 31–84, syntaxin residues 196–255, and SNAP-25 residues 23–78 and 147–200, and superposition was carried out for the endosomal structure using endobrevin residues 11–64, syntaxin 7 residues 169–228, vti1b residues 140–195, and syntaxin-8 residues 152–205. r.m.s.d., root mean square difference.

Structure 1	Structure 2	C_α r.m.s.d.(Å)
Microcomplex	Endosomal complex	1.619
Microcomplex	Minimal complex	0.947 (Molecule 1)
		0.724 (Molecule 2)
		1.139 (Molecule 3)
Endosomal complex	Minimal complex	1.187 (Molecule 1)
		1.270 (Molecule 2)
		1.087 (Molecule 3)

thermal stability of the various SNARE complexes under native conditions by CD. Both the minimal and the N-terminally truncated SNARE complexes have a T_m of 94 °C, whereas the micro-SNARE complex has a reduced T_m of 89 °C (Fig. 2*b*).

Synaptotagmin Binding—Having demonstrated that the micro-SNARE complex forms a quantitative and stable complex, albeit with somewhat reduced T_m, we investigated whether it would retain its ability to interact with the C_2 domains of synaptotagmin I. GST pull-down experiments were conducted in the presence of both 1 mM EDTA and 0.5 mM $CaCl_2$. As shown in Fig. 3, synaptotagmin I is capable of binding the micro-SNARE complex in both the presence and absence of Ca^{2+}. These findings are consistent with prior reports using the C_2AB domain of synaptotagmin III and the minimal SNARE complex (37).

Microcomplex Structure—We next determined the crystal structure of the microcomplex. Crystals were obtained in space group $P2_12_12_1$ in the presence of MPD and $CaCl_2$ at 4 °C. These conditions are similar to the previous crystallization conditions used for the minimal SNARE complex (9). The crystal structure contained only one copy of the complex per asymmetric unit in contrast to the minimal SNARE complex that crystallized in a different space group (I222) with three complexes per asymmetric unit. Most importantly, the crystals of the microcomplex diffracted to 1.4 Å, making this the highest resolution crystal structure of a SNARE complex available to date. All of the residues of the microcomplex were visible in the final model, which refined to a R_{cryst} value of 19.8% and a R_{free} value of 22.4%. The statistics of the diffraction data and the final refined model are shown in Tables I and II. The electron density maps are of excellent quality (Fig. 5*b*) and allowed assignments of nearly all of the side-chain rotamers.

Three Ca^{2+} sites were found that are coordinated by symmetry-related molecules. These sites were visible as 8 σ peaks in $2F_o - F_c$ maps. The coordinating oxygen atoms are located on SNAP-25 Gln-20 and Glu-27 of a SNARE complex and synaptobrevin Asp-80, Lys-83 of SNAP-25, Tyr-88, Trp-89, and syntaxin Lys-256 of a symmetry-related complex. Several water molecules complete the coordination spheres around the Ca^{2+}. Because these Ca^{2+} sites are located at the artificially truncated C terminus of the microcomplex, it is probable that these binding sites are the result of crystallization conditions.

As expected, the micro-SNARE complex forms a four-helix bundle. The C_α atoms of the microcomplex were superimposed on that of the minimal complex structure and on all of the homologous residues of the endosomal complex structure. The results of these superpositions are shown in Fig. 4, *a* and *b*, and Table III. It is interesting to note that the root mean square (r.m.s) difference between the microcomplex structure and the endosomal structure is larger than the root mean square dif-
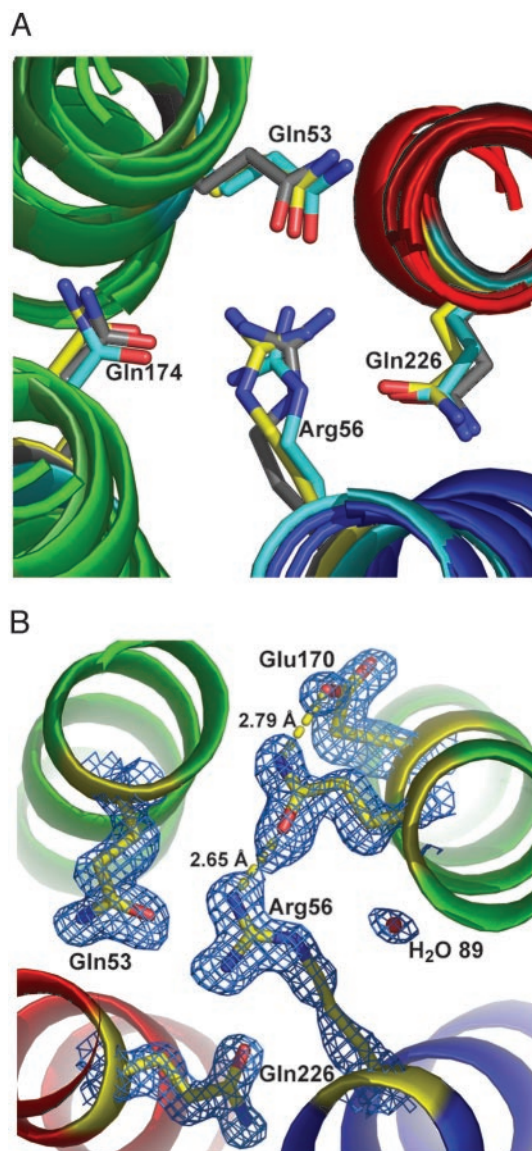

FIG. 5. **Ionic central layer.** *A*, alternate conformations of synaptobrevin Arg-56 at the ionic central layer. Residues for the microcomplex structure are shown in *yellow*, residues for the minimal complex (chains *a–d*) are shown in *cyan*, and residues for the endosomal structure are shown in *gray*. Residues are numbered according to the sequences of the neuronal SNARE complex. *B*, electron density at the ionic central layer of the micro-SNARE complex. Shown is a $2F_o - F_c$ σ_A-weighted omit map. The electron density is contoured at 1.5 σ. Synaptobrevin is shown in *blue*, syntaxin is shown in *red*, and SNAP-25 is shown in *green*.

ference observed when comparing either structure to the minimal complex structure. In contrast to the endosomal structure, the microcomplex displays little variation in *B*-values over most of the four-helix bundle (see Fig. 4*c*). Only the second α-helix of SNAP-25 between layers 2 and 8 and synaptobrevin between layers −7 and 0 display any systematic increase in C_α *B*-values.

To further compare the various SNARE complex crystal structures, we superimposed the residues around the ionic central layer (Fig. 1) with the corresponding residues of the previously solved structures. For the neuronal SNAREs, the layer consists of synaptobrevin Arg-56, syntaxin Gln-226, SNAP-25 Gln-53, and SNAP-25 Gln-174. For the endosomal complex, the corresponding residues are endobrevin Arg-76, syntaxin-7 Gln-199, vti1b Gln-170, and syntaxin-8 Gln-179. The root mean square differences for residues at this layer between the microcomplex and the endosomal complex are

0.315 and 0.509 Å for C_α and all atoms, respectively. Several of the SNARE crystal structures show the presence of a bifurcated hydrogen bond between synaptobrevin Arg-56 and SNAP-25 Gln-53 and Gln-174 (Fig. 5*a*). However, in one of the molecules of the minimal complex crystal structure (Fig. 5*a*, *cyan*), Arg-56 exhibits a rotamer that allows direct hydrogen bonding from each of the side-chain nitrogen atoms of Arg-56 to each of the buried glutamines. This Arg-56 rotamer is also visible in the structure of the squid neuronal SNARE complex with complexin (38). Thus, Arg-56 exhibits significant conformational variability among the different structures, whereas the three glutamines exhibit very similar conformations (Fig. 5*a*). The observed conformational variability of the central layer may suggest a possible functional role in the disassembly process (39).

The quality of our diffraction data allowed us to assign numerous sites of hydration that were previously unobservable (Fig. 5*b*). Of particular interest is a buried water molecule (Fig. 5*b*, H_2O 89) at the ionic central layer. This water molecule is located 3.10 Å from the ϵ-nitrogen of Arg-56, satisfying the hydrogen bond requirements of this nitrogen. It is possible that this water molecule is not present when Arg-56 adopts alternate conformations observed in some of the other crystal structures.

The formation of salt bridges on the surface of proteins is known to stabilize exposed structural elements. The presence of surface salt bridges positioned to stabilize buried structural elements is less common. However, a carboxylic acid ϵ-oxygen of SNAP-25 Glu-170 shows just such an interaction buttressing SNAP-25 Gln-174 at 2.79 Å through the Gln-174 ϵ-nitrogen (Fig. 5*b*). This interaction stabilizes the SNAP-25 Gln-174 ϵ-oxygen, which in turn interacts with synaptobrevin Arg-56 Nη2 at a distance of 2.65 Å (Fig. 5*b*). The close interaction of synaptobrevin Arg-56 Nη2 with the SNAP-25 Gln-174 ϵ-oxygen as compared with the Arg-56 Nη1 and syntaxin Gln-226 interaction probably reflects the proximity of the negatively charged carboxylic group from SNAP-25 Glu-170. We note further that SNAP-25 Glu-170 is a highly conserved residue in the SNAP-25 family, including the endosomal SNARE syntaxin-8.

DISCUSSION

The neuronal SNARE complex can form oligomers under various conditions (18, 44). We have shown that C-terminal truncation of synaptobrevin, C-terminal to residue 89 (see Fig. 1), along with C-terminal truncation of syntaxin produces a SNARE complex that is both monomeric and monodisperse. Interestingly, the fragments of synaptobrevin containing residues 77–90 bind to phospholipids (40, 41). Thus, it is possible that some of the residues that are involved in phospholipids binding are also involved in oligomerization.

We have shown that C-terminal truncation but not N-terminal truncation of the minimal SNARE complex results in a reduction in stability as measured by CD and SDS thermal melts. Other investigators have used SDS stability to characterize various combinations of SNARE proteins (42). Thus, considering the influence on stability by the C-terminal end of the SNARE complex, a comparison of SDS stability should be viewed with caution when comparing the stabilities of various SNARE combinations.

Our finding that the microcomplex retains the ability to bind synaptotagmin is particularly noteworthy in view of the recent discovery of DNA contaminants and sequence mutations in earlier binding studies with synaptotagmin I C_2AB (19). Thus, SNARE binding by synaptotagmin is independent of oligomerization of the SNARE complex.

Through C-terminal truncation, we obtained a microcomplex that allowed us to solve the structure of the SNARE complex at near atomic resolution. The structure confirmed many of the observations that we reported in our previous 2.4-Å structure (9). The structure also revealed several new details of the SNARE complex. The existence of alternate conformations of the buried arginine at the ionic central layer is consistent with a function for this layer in NSF-mediated disassembly of the SNARE complex (17). Previously, unobservable interactions included a buried water molecule and a salt bridge that were likely to play an important role in stabilizing the ionic central layer (Fig. 5*b*). Such structural details offer important new information for the design of future experiments to study SNARE complex function.

REFERENCES

1. Söllner, T., Bennett, M. K., Whiteheart, S. W., Scheller, R. H., and Rothman, J. E. (1993) *Cell* **75,** 409–418
2. Weber, T., Zemelman, B. V., McNew, J. A., Westermann, B., Gmachl, M., Parlati, F., Söllner, T. H., and Rothman, J. E. (1998) *Cell* **92,** 759–772
3. Bennett, M. K., Calakos, N., and Scheller, R. H. (1992) *Science* **257,** 255–259
4. Calakos, N., Bennett, M. K., Peterson, K. E., and Scheller, R. H. (1994) *Science* **263,** 1146–1149
5. Blasi, J., Chapman, E. R., Link, E., Binz, T., Yamasaki, S., De Camilli, P., Südhof, T. C., Niemann, H., and Jahn, R. (1993) *Nature* **365,** 160–163
6. Ferro-Novick, S., and Jahn, R. (1994) *Nature* **370,** 191–193
7. Südhof, T. C. (1995) *Nature* **375,** 645–653
8. Fernández-Chacón, R., Königstorfer, A., Gerber, S. H., Garcia, J., Matos, M. F., Stevens, C. F., Brose, N., Rizo, J., Rosenmund, C., and Südhof, T. C. (2001) *Nature* **410,** 41–49
9. Sutton, R. B., Fasshauer, D., Jahn, R., and Brunger, A. T. (1998) *Nature* **395,** 347–353
10. Trimble, W. S., and Scheller, R. H. (1988) *Trends Neurosci.* **11,** 241–242
11. Baumert, M., Maycox, P. R., Navone, F., De Camilli, P., and Jahn, R. (1989) *EMBO J.* **8,** 379–384
12. Bennett, M. K., Garcia-Arraras, J. E., Elferink, L. A., Peterson, K., Fleming, A. M., Hazuka, C. D., and Scheller, R. H. (1993) *Cell* **74,** 863–873
13. Fernandez, I., Ubach, J., Dulubova, I., Zhang, X., Südhof, T. C., and Rizo, J. (1998) *Cell* **94,** 841–849
14. Oyler, G. A., Higgins, G. A., Hart, R. A., Battenberg, E., Billingsley, M., Bloom, F. E., and Wilson, M. C. (1989) *J. Cell Biol.* **109,** 3039–3052
15. Vogel, K., Cabaniols, J. P., and Roche, P. A. (2000) *J. Biol. Chem.* **275,** 2959–2965
16. Wei, S., Xu, T., Ashery, U., Kollewe, A., Matti, U., Antonin, W., Rettig, J., and Neher, E. (2000) *EMBO J.* **19,** 1279–1289
17. Scales, S. J., Yoo, B. Y., and Scheller, R. H. (2001) *Proc. Natl. Acad. Sci. U. S. A.* **98,** 14262–14267
18. Fasshauer, D., Eliason, W. K., Brunger, A. T., and Jahn, R. (1998) *Biochemistry* **37,** 10354–10362
19. Ubach, J., Lao, Y., Fernandez, I., Arac, D., Südhof, T. C., and Rizo, J. (2001) *Biochemistry* **40,** 5854–5860
20. Ausubel, F. M., Brent, R., Kingston, R. E., Moore, D. D., Seidman, J. G., Smith, J. A., and Struhl, K. (1998) in *Current Protocols in Molecular Biology* (Chanda, V. B., ed), Vol. 1, pp. 1.1–1.8, John Wiley & Sons, Inc., New York
21. Coligan, J. E., Dunn, B. M., Ploegh, H. L., Speicher, D. W., and Wingfield, P. T. (2000) in *Current Protocols in Protein Science*, Vol. 1, pp. 5.1–5.3, John Wiley & Sons, Inc., New York
22. Wyatt, P. (1993) *Anal. Chim. Acta* **272,** 1–40
23. Otwinowski, Z., and Minor, W. (1997) *Methods Enzymol.* **276,** 307–325
24. DeLano, W. L., and Brunger, A. T. (1995) *Acta Crystallogr. Sec. D* **51,** 740–748
25. Brunger, A. T., Adams, P. D., Clore, G. M., DeLano, W. L., Gros, P., Grosse-Kunstleve, R. W., Jiang, J. S., Kuszewski, J., Nilges, M., Pannu, N. S., Read, R. J., Rice, L. M., Simonson, T., and Warren, G. L. (1998) *Acta Crystallogr. Sec. D* **54,** 905–921
26. Jones, T. A., Zou, J. Y., Cowan, S. W., and Kjeldgaard, M. (1991) *Acta Crystallogr. Sec. A* **47,** 110–119
27. Rice, L. M., and Brunger, A. T. (1994) *Proteins* **19,** 277–290
28. Hendrickson, W. A. (1985) *Methods Enzymol.* **115,** 252–270
29. Adams, P. D., Pannu, N. S., Read, R. J., and Brunger, A. T. (1997) *Proc. Natl. Acad. Sci. U. S. A.* **94,** 5018–5023
30. Brunger, A. T. (1992) *Nature* **355,** 472–475
31. Kleywegt, G. J. (1996) *Acta Crystallogr. Sec. D* **52,** 842–857
32. DeLano, W. L. (2002) *The PyMOL Molecular Graphics System*, version 0.8, DeLano Scientific (www.pymol.org), San Carlos, CA
33. Nicholls, A., Sharp, A., and Honig, B. (1991) *Proteins Struct. Funct. Genet.* **11,** 281–296
34. Margittai, M., Fasshauer, D., Pabst, S., Jahn, R., and Langen, R. (2001) *J. Biol. Chem.* **276,** 13169–13177

35. Antonin, W., Holroyd, C., Tikkanen, R., Honing, S., and Jahn, R. (2000) *Mol. Biol. Cell* **11,** 3289–3298
36. Fasshauer, D., Sutton, R. B., Brunger, A. T., and Jahn, R. (1998) *Proc. Natl. Acad. Sci. U. S. A.* **95,** 15781–15786
37. Sutton, R. B., Ernst, J. A., and Brunger, A. T. (1999) *J. Cell Biol.* **147,** 589–598
38. Bracher, A., Kadlec, J., Betz, H., and Weissenhorn, W. (2002) *J. Biol. Chem.* **277,** 26517–26523
39. Scales, S. J., Finley, M. F., and Scheller, R. H. (2001) *Science* **294,** 1015–1016
40. Quetglas, S., Iborra, C., Sasakawa, N., De Haro, L., Kumakura, K., Sato, K., Leveque, C., and Seagar, M. (2002) *EMBO J.* **21,** 3970–3979
41. Quetglas, S., Leveque, C., Miquelis, R., Sato, K., and Seagar, M. (2000) *Proc. Natl. Acad. Sci. U. S. A.* **97,** 9695–9700
42. Foster, L. J., Yeung, B., Mohtashami, M., Ross, K., Trimble, W. S., and Klip, A. (1998) *Biochemistry* **37,** 11089–11096
43. Chen, Y. A., Scales, S. J., Duvvuri, V., Murthy, M., Patel, S. M., Schulman, H., and Scheller, R. H. (2001) *J. Biol. Chem.* **276,** 26680–26687
44. Hua, Y., and Scheller, R. H. (2001) *Proc. Natl. Acad. Sci. U. S. A.* **98,** 8065–8070